IOSR Journal of Mathematics (IOSR-JM)
e-ISSN: 2278-5728, p-ISSN: 2319-765X. Volume 19, Issue 3 Ser. I (May. – June. 2023), PP 51-70
www.iosrjournals.org

Numerical Study of Blood Flow Using Oldroyd-B Fluids in Various Aneurysmatic Arteries Conditions

Mohammed Nasir Uddin[*1]
[1]*Department of Information and Communication Technology (ICT), Bangladesh University of Professionals (BUP), Dhaka-1216, Bangladesh*

Abstract:
Blood flow is analyzed for various aneurysmatic arteries of the regular tissue using Oldroyd-B fluid. A finite element method is used to analyze blood flow numerically for the different situations of aneurysmatic arteries. The Oldroyd-B fluid is considered due to the manner of blood viscosity. In this paper, the impact of an aneurysm artery on blood flow in various arterial conditions has been studied. The Oldroyd-B model has been used to study the blood flow characteristics in bulge arteries. The non-linear partial differential equations are converted into dimensionless equations using non-dimensional variables and solved mathematically. The uniqueness of this study is to determine the arterial diseases for aneurysmatic arteries with various conditions. The impact of 100% aneurysm artery on the blood flow is an important result to identify cardiovascular diseases. The highest effect of pressure on blood flow is a remarkable finding of this work. The blood flow has been affected by the Reynolds number and it has changed the blood flow pattern at dilating region significantly. The simulation of blood velocity and pressure is shown through the contour lines and streamlines. In this study, the main changes in blood flow characteristics are found due to the presence of different aneurysmatic arteries condition. The outcomes of this study can be used to know the arterial diseases and enhance the understanding level of various situations of aneurysmal artery which may help to explore the knowledge of medical research. The velocity and pressure profiles of blood flow are shown graphically for Oldroy-B fluid.

Keywords: *Aneurysmatic artery; Oldroyd-B fluid; Finite element method; Blood flow; Viscoelasticity*

Date of Submission: 20-05-2023 Date of Acceptance: 30-05-2023

I. Introduction

An aneurysm is defined as an abnormal bulging and weakened area in the wall of a blood vessel involving an expansion in diameter above 50 percent compared with the expected normal width[1]. As a result, irregular growth or weakened blood vessel wall are found which is bubble or balloon shaped. Abdominal Aortic aneurysm, Cerebral aneurysm, iliac aneurysm and Peripheral aneurysm are commonly found in the human body**.** A rupture in an artery leads to life-threatening uncontrolled bleeding and it may result in possibly death. The main causes and nature of aneurysms are still an important subject of debate and almost 75 % of patients with aneurysms die before reaching the hospital. At present bioengineers, medical researchers, and scientists are more interested to do the study of blood flow due to its significant effect on various human arterial diseases such as Bleeding, Atherosclerosis, Stroke, Congenital disorders, kidney damage, and high blood pressure. The hemodynamical features refer to basic measures of cardiovascular function that can change the rheological properties during the blood circulation system. It plays an important role to the expansion and progression of various cardiovascular diseases [2] [3]. In the case of arterial diseases and aneurysms, the blood circulation system is confined and originates disorder in the human blood flow system. So, flowing blood loses it natural behavior and develops non-Newtonian fluid. Now, A good number of researchers [4-6] have investigated aneurysms with different perspectives and still have a huge prospect to contribute in the sector. It is essential to find out the major factors that are mainly responsible of the increase of abnormal aneurysms and ruptures.

The study of the aneurysmal artery is essential to know the blood behavior characteristics through the dilated blood vessel as the wall shear stress, pressure decline, and velocity change are some vital factors to detect arterial diseases [7-9]. Finol and Amon [6] have studied a mathematical forecast of blood flow patterns and hemodynamic stresses for two aneurysms with distinct sizes in abdominal aortic aneurysms. Elia et al. [10] have discussed the numerical simulation of blood flow in 2D idealized stenosis artery for capturing the shear-thinning rheological behavior by applying the data assimilation method. A blood flow analysis has been done for numerical simulation by Prokop and Kozel [11] for generalized Newtonian and Oldroyd-B models. Telma et. al [12] have studied the blood simulations by including known data. An analysis of aneurysmal hemodynamics has been done for laminar blood flow [13] and has shown the effect of an aneurysm artery on recirculating vortex. It has been

examined by Mukhopadhyay and Layek [14] that the systematic assessment of blood flow in the existence of hematocrit at local aneurysm. In a bulge blood vessel, the pulsatile suspension flow of blood with hemodynamic properties has been studied [15]. The wall shear stress is assessed for thoracic aortic aneurysms and shown that the devices are very effective for treatment methods at arterial disease [16]. Ramella et al. [16] have shown the changes in abdominal aortic aneurysms and found the effect of cyclic stretch on vascular endothelial cells and abdominal aortic aneurysms. Stergiou et. al [17] have studied the aneurysmal artery and identified the effect of hematocrit performances on blood flow using the Fluid-Structure Interaction method. They have said that the dynamic behavior in an abdominal aneurysm artery and the deviation of blood viscosity are correlated to hematocrit value.

Recently, a study of blood flow in aneurysm models has been examined [18] and observed that the hemodynamics movement of blood flow is influenced by the different models of the aneurysmal artery. An investigation has been done by Shafii et. al [19] for hemodynamic and blood flow recirculation effect on rupture prediction of centre cerebral artery aneurysm. A review has studied on the effects of blood flow patent and cross-sectional area on hemodynamic into patient-specific cerebral aneurysm via fluid-structure interaction method [20]. Lindquist et. al [21] have shown that a geometric and biomechanical modeling aided by machine learning progresses the forecast of expansion and rupture of small abdominal aortic aneurysms. Uddin et al. [22] have studied the permeable aneurysmal effect on blood flow in human bodies. They have observed a significant change in the presence of permeability in aneurysmal arteries for Newtonian, Oldroyd-B fluid, and generalized Newtonian and Oldroyd-B fluid. A numerical study has been achieved to know the effect of blood flow properties due to the existence of rupture in the cerebral aneurysm by Shen et al. [23]. They observed that the incoming bloodstream with inclination is significantly effective in the aneurysmal area. Shen et al. [24] have investigated the simulation of blood flow for the dilating aneurysm in the middle cerebral artery. A comparative numerical study [25] of blood flow has been done for stenotic and aneurysmatic arteries with the existence and non-existence of blood clots.

With the above encouragement, an endeavor is made in the present numerical analysis to study an aneurysmatic artery with various conditions for Oldroyd-B fluid. A generalized cross-model is used for blood flow analysis. In this work, the main physiological significance and more focus are given to demonstrate the main variations in the presence of different aneurysmal arteries are considered models.

In this study, a mathematical study of blood flow with various sizes of aneurysmal arteries has been discussed to explore the effects of dilating blood vessels and the Reynold numbers for Oldroyd-B cases. An analysis and simulation of blood flow are shown for different sizes of aneurysms, and it is presented graphically for the Oldroyd-B case. The mathematical equations of blood flow are considered for 2D steady case and then a finite element model has been developed for the present problem.

II. Mathematical Formulation

The expanded blood vessel portion having various types of aneurysmal artery is modeled and steady 2D viscoelastic fluid with incompressible non-Newtonian fluid is characterized by a generalized cross model. The model in the present study is shown in Figure 1 and Figure 2 is the main interest for considering the present model. The parabolic velocity profile is considered at the inlet and the rigid wall is considered to avoid the complexity of the constitutive equations. An arterial model has been used [26] for multiple stenoses. The present mathematical structure of the geometrical model for multiple aneurysms is shown in Figure 1.

$$h_a = \frac{R(x)}{R_0(x)}$$

$$= \begin{cases} 1 + \dfrac{\varepsilon}{2R_0 l_a^4}\{11(x-l_0)\,l_a^3 - 47(x-l_0)^2\,l_a^2 + 72(x-l_0)^3 l_a - 36(x-l_0)^4\},\ l_0 \le x \le l_0 + l_a \\ 1,\ otherwise \end{cases} \quad (1)$$

Where R(x) is the radius of aneurysmatic region, R_0(x) denotes the radius of non-aneurysmatic section, l_a is the length of aneurysm, and l_0 is the dilating location, ε is the maximum height of the aneurysm. The aneurysm positions are at x =l_0+l_a/6 and x =l_0+5l_a/6 respectively. The critical height is taken as 3ε/4 at x=l_0 +l_a/2 from the origin.

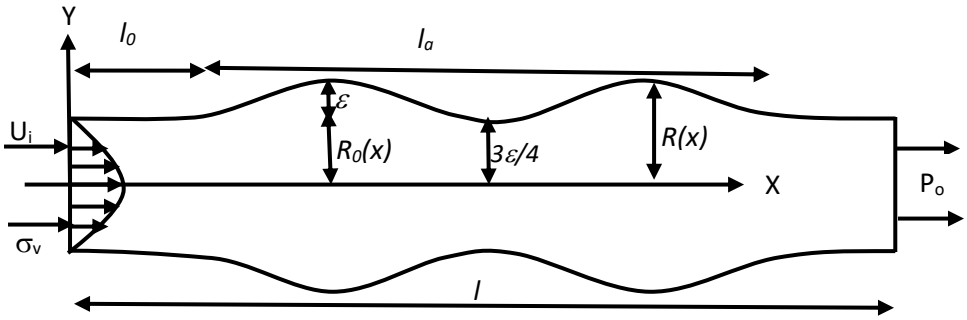

Figure 1. Multiple aneurysmatic artery

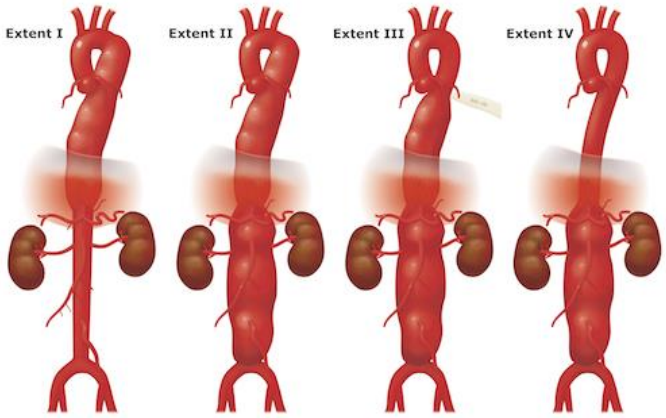

Figure 2. View of multiple aortic aneurysm [27]

III. Mathematical model

Consider the blood flow in the multiples aneurysmal artery to be two-dimensional, laminar, symmetrical, and fully developed. The generalized cross model is used for blood flow due to the properties of viscoelastic and shear-thinning. The governing mathematical equations [28] [29] of blood flow are as follows in vector form:

Continuity Equation:

$$\nabla . u = 0 \tag{1}$$

Momentum Equation:

$$\rho \frac{\partial \boldsymbol{u}}{\partial t} + \rho(u.\nabla)\boldsymbol{u} = -\nabla p + \mu_n \Delta \boldsymbol{u} + \nabla . \sigma + \rho f \tag{2}$$

Oldroyd-B Constitutive Equation:

$$\sigma + \lambda_x[\frac{\partial \sigma}{\partial t} + (\boldsymbol{u}.\nabla)\sigma] = 2\mu_v \boldsymbol{V}(\boldsymbol{u}) + \lambda_x[\sigma V^{/} - V^{/}\sigma - \sigma V - V\sigma] \tag{3}$$

Where, the velocity vector, $\boldsymbol{u}= (u_1, u_2, u_3)^T$, ρ denotes the density, the stress tensor, $\boldsymbol{\sigma}=2\mu\boldsymbol{V}$, μ is dynamic viscosity, **V** is the velocity gradient, and λ_x is the relaxation. The total viscosity $\mu= \mu_n + \mu_v$, where Newtonian viscosity is μ_n and viscoelasticity is μ_v. If the relaxation (λ_x) and retardation time (λ_d) then $\frac{\lambda_d}{\lambda_x} = \frac{\mu_n}{\mu_n+\mu_v}$. The generalized Cross model [12] [30] considered for the blood viscoelasticity behavior as follows:

$$\mu(\dot{\gamma}) = \mu_\infty + \frac{\mu_0 - \mu_\infty}{(1+(\lambda\dot{\gamma})^b)^a} \tag{4}$$

with the parameters a, b, λ>0.

Applying the following dimensionless variables to form dimensionless equations.

$x=LX$, $y=LY$, $t = Lt^*/U$, $\boldsymbol{u} = UU_o$, $\boldsymbol{v} = VU_o$ $p = \mu UP/L$, $\sigma= U\mu\sigma^*/L$, $f = f^*\mu U/L^2$, $\nabla= \nabla^*/L$, $Wi = \lambda_x U/L$, $Re= \rho UL/\mu$.

Where, X and Y are the dimensionless quantities along x and y axis respectively. U and V are velocity components U and V are considered along horizontal and vertical axes respectively, P denotes pressure, L is characteristics length, σ^* is stress tensor, and Weissenberg number (Wi), Reynold number (Re) are dimensionless numbers. The dimensionless governing equations are as follows:

Continuity Equation:

$$\nabla . U = 0 \tag{5}$$

Momentum Equations:

$$Re[(\boldsymbol{U}.\nabla)\boldsymbol{U}] = -\nabla P + (1-\lambda)\Delta \boldsymbol{U} + \nabla . \boldsymbol{\sigma} + f \tag{6}$$

Oldroyd-B constitutive equation:

$$W_i[(\mathbf{U}.\nabla)\boldsymbol{\sigma}]+\boldsymbol{\sigma}=2\mu_v\mathbf{V}(\mathbf{U})+W_i[(\nabla\mathbf{U})\boldsymbol{\sigma}+\boldsymbol{\sigma}(\nabla\mathbf{U})^t] \quad (7)$$

Boundary conditions

The boundary conditions are required to solve the governing equations and three disjoint parts of the boundary wall are inflexible wall, outlet, and inlet. The following boundary conditions are considered for the present study

(a) At inlet:

The axial velocity profile at inlet is $\boldsymbol{u} = 1.5\,U_i(1-y^2)$, $\boldsymbol{v} = 0$ and the corresponding extra stresses components are $\sigma_{11} = 2\mu_v Wi(\frac{\partial u}{\partial y})^2$, $\sigma_{12} = \mu_v \frac{\partial u}{\partial y}$, $\boldsymbol{\sigma}_{22} = 0$

Where, y is along the inlet boundary, and U_i is the mean blood velocity.

(b) At outlet:

Pressure force (P_o) is considered at the boundary, $\boldsymbol{\sigma}.\boldsymbol{n} = -P_o\boldsymbol{n}$ and homogeneous Neumann conditions is fixed for velocity components and uniform pressure is given.

(c) At boundary wall:

No-slip homogeneous Dirichlet conditions, $\boldsymbol{u} = 0$, $(\boldsymbol{\sigma}.\boldsymbol{n}).\boldsymbol{n} = 0$ and homogenous Neumann boundary conditions are set for the pressure.

In this study, the continuity equation (5), momentum equation (6), Oldroyd-B equation (7) are considered to account for blood viscoelasticity.

IV. Numerical Analysis

The governing differential equations have been solved for the dependent variables such as velocity, pressure and stress tensor using the boundary conditions. The finite element method [31] [32] and Mathematical programming package COMSOLMULTIPHYSICS [33] have been used to solve this problem. PDE solver MATLAB programing [34] is used for as a Newton-Raphson iteration technique. The velocity and viscoelasticity Equations (8-10) result in a set of non-linear coupled equations for which an iterative scheme is adopted. the velocity are found from equations (5) and (6) and then compute the pressure using $p = 2\mu_s\boldsymbol{V}(u) + T + \sigma$. The numerical technique [35][36] have been done based on the Galerkin-weighted residual method for finite element formulation and details are given here below. The weighted residual method is applied then

$$\int_A N_\alpha(\nabla.U)\,\mathrm{dA} = 0 \quad (8)$$

$$Re\int_A N_\alpha U(\nabla.U)dA = -\int_A H_\lambda\nabla P\,dA + \int_A N_\alpha\nabla\sigma\,dA + (1-\lambda)\int_A N_\alpha\nabla^2U\,dA + \int_A N_\alpha f\,dA \quad (9)$$

$$Re\int_A N_\alpha U(\nabla.V)\,dA = -\int_A H_\lambda\nabla P\,dA + \int_A N_\alpha\,\nabla\sigma dA + (1-\lambda)\int_A N_\alpha\nabla^2V\,dA + \int_A N_\alpha f\,dA \quad (10)$$

$$W_i\int_A N_\alpha U(\nabla.\sigma)\,dA + \int_A N_\alpha\sigma\,dA = \int_A \mu_v N_\alpha(\nabla.U)\,dA + W_i\int_A N_\alpha(\nabla.U)\sigma + \sigma(\nabla.U)\,dA \quad (11)$$

Now use Gauss's theorem to form the boundary integral terms connected with the surface tractions, extra-stress tensor then

$$Re\int_A N_\alpha U(\nabla.U)\,dA + \int_A H_\lambda\nabla P\,dA - \int_A N_\alpha\nabla.\sigma\,dA - (1-\lambda)\int_A N_\alpha\nabla^2U\,dA - \int_A N_\alpha f_x\,dA = \int_{s_0} N_\alpha S_x\,ds_0 \quad (12)$$

$$Re\int_A N_\alpha U(\nabla.V)\,dA + \int_A H_\lambda\nabla P\,dA - \int_A N_\alpha\nabla\sigma\,dA - (1-\lambda)\int_A N_\alpha\nabla^2V\,dA - \int_A N_\alpha f_y\,dA = \int_{s_0} N_\alpha S_y\,ds_0 \quad (13)$$

$$W_i\int_A N_\alpha U.(\nabla\sigma)\,\mathrm{dA} + \int_A N_\alpha\sigma\,\mathrm{dA} - \int_A \mu_v N_\alpha\nabla.U\,\mathrm{dA} - W_i\int_A N_\alpha[(\nabla.U)\sigma + \sigma(\nabla.U)]\,\mathrm{dA} = \int_A N_\alpha\sigma_w\,\mathrm{ds}_w \quad (14)$$

The six-node triangular element are considered to form finite element equations. All six nodes are allied with velocities and stress tensors; only the corner nodes are connected with pressure. So, a lower-order polynomial is chosen for pressure so that it satisfies the continuity equation. The elementary unknown variables are the velocity components *U*, *V* the stress tensor, σ and the pressure, *P* of the partial differential equations. The following equations are taken on the base of the maximum orders of the differential Equations (5-7) for the velocity component and the stress tensor distributions and linear interpolation for the pressure distribution.

$$U(X,Y) = N_\alpha U_\alpha \quad (15)$$

$$V(X,Y) = N_\alpha V_\alpha \quad (16)$$

$$\sigma(X,Y) = N_\alpha\sigma_\alpha \quad (17)$$

$$P(X,Y) = H_\lambda P_\lambda \quad (18)$$

The velocity interpolation functions are N_α (α = 1, 2, … …, 6), the pressure interpolation functions are H_λ(λ= 1, 2, 3), Applying the equations (15-18) in the equations (5-7) then the finite element equations can be written as follows

$$K_{\alpha\beta^x}U_\beta + K_{\alpha\beta^y}V_\beta = 0 \quad (19)$$

$$Re(K_{\alpha\beta\gamma^x}U_\beta U_\gamma + K_{\alpha\beta\gamma^y}V_\beta U_\gamma) + M_{\alpha\mu^x}P\mu + K_{\alpha\beta^x}\sigma_\beta + K_{\alpha\beta^y}\sigma_\beta$$

$+(1-\lambda)(S_{\alpha\beta^{xx}}+S_{\alpha\beta^{yy}})U_\beta - f_x K_\alpha = Q_{\alpha^u}$ (20)

$Re(K_{\alpha\beta\gamma^x}U_\beta V_\gamma + K_{\alpha\beta\gamma^y}V_\beta V_\gamma) + M_{\alpha\mu^y}P_\mu + K_{\alpha\beta^x}\sigma_\beta$
$+K_{\alpha\beta^y}\sigma_\beta + (1-\lambda)(S_{\alpha\beta^{xx}}+S_{\alpha\beta^{yy}})V_\beta - f_y K_\alpha = Q_{\alpha^v}$ (21)

$W_i(K_{\alpha\beta\gamma^x}U_\beta\sigma_\gamma + K_{\alpha\beta\gamma^y}V_\beta\sigma_\gamma) + K_{\alpha\beta}\sigma_\mu - \mu_v(K_{\alpha\beta^x}U_\alpha + K_{\alpha\beta^y}U_\beta)$
$-W_i\left(K_{\alpha\beta\gamma^x}U_\beta\sigma_\gamma + K_{\alpha\beta\gamma^y}U_\beta\sigma_\gamma\right) = Q_{\alpha^T}$ (22)

Where, the coefficients in element matrices are in the form of the integrals over the element area and along the element edges S_0 and S_w as,

$K_\alpha = \int_A N_\alpha\, dA$, $K_{\alpha\beta^x} = \int_A N_\alpha N_{\beta,x} dA$, $K_{\alpha\beta^y} = \int_A N_\alpha N_{\beta,y} dA$, $K_{\alpha\beta\gamma^x} = \int_A N_\alpha N_\beta N_{\gamma,x} dA$,
$K_{\alpha\beta\gamma^y} = \int_A N_\alpha N_\beta N_{\gamma,y} dA$, $K_{\alpha\beta} = \int_A N_\alpha N_\beta dA$, $S_{\alpha\beta^{xx}} = \int_A N_{\alpha,x} N_{\beta,x} dA$,
$S_{\alpha\beta^{yy}} = \int_A N_{\alpha,y} N_{\beta,y} dA$, $M_{\alpha\mu^x} = \int_A H_\alpha H_{\mu,x} dA$, $M_{\alpha\mu^y} = \int_A H_\alpha H_{\mu,y} dA$, $Q_{\alpha^u} = \int_{S_0} N_\alpha S_x dS_0$,
$Q_{\alpha^v} = \int_{S_0} N_\alpha S_y dS_0$, $Q_{\alpha^\sigma} = \int_{S_0} N_\alpha \sigma_w dS_w$

Applying the Newton-Raphson iteration technique to the set of nonlinear algebraic Equations (19-22) are transferred into linear algebraic equations. Finally, these linear equations are solved by applying the triangular factorization method and reduced integration technique of [37] and the finite element Equations (19-22) as,

$F_{\alpha^p} = K_{\alpha\beta^x}U_\beta + K_{\alpha\beta^y}V_\beta$ (23)

$F_{\alpha^u} = Re(K_{\alpha\beta\gamma^x}U_\beta U_\gamma + K_{\alpha\beta\gamma^y}V_\beta U_\gamma) + M_{\alpha\mu^x}P\mu - K_{\alpha\beta^x}\sigma_\beta - K_{\alpha\beta^y}\sigma_\beta$
$+(1-\lambda)(S_{\alpha\beta^{xx}}+S_{\alpha\beta^{yy}})U_\beta - f_x K_\alpha - Q_{\alpha^u}$ (24)

$F_{\alpha^v} = Re(K_{\alpha\beta\gamma^x}U_\beta V_\gamma + K_{\alpha\beta\gamma^y}V_\beta V_\gamma) + M_{\alpha\mu^y}P_\mu - K_{\alpha\beta^x}\sigma_\beta - K_{\alpha\beta^y}\sigma_\beta$
$+(1-\lambda)(S_{\alpha\beta^{xx}}+S_{\alpha\beta^{yy}})V_\beta - f_y K_\alpha - Q_{\alpha^v}$ (25)

$F_{\alpha^\sigma} = W_i(K_{\alpha\beta\gamma^x}U_\beta\sigma_\gamma + K_{\alpha\beta\gamma^y}V_\beta\sigma_\gamma) + K_{\alpha\beta}\sigma_\beta - \mu_v(K_{\alpha\beta^x}U_\beta + K_{\alpha\beta^y}V_\beta)$
$-2W_i\left(K_{\alpha\beta\gamma^x}U_\gamma\sigma_\beta + K_{\alpha\beta\gamma^y}U_\gamma\sigma_\beta\right) - Q_{\alpha^\sigma}$ (26)

A set of algebraic equations with the incremental unknowns variables of the element's nodal velocity components, temperatures, and pressures in the form,

$$\begin{bmatrix} K_{uu} & K_{uv} & K_{u\sigma} & K_{u\theta} & K_{up} \\ K_{vu} & K_{vv} & K_{v\sigma} & K_{v\theta} & K_{vp} \\ K_{\sigma u} & K_{\sigma v} & K_{\sigma\sigma} & 0 & 0 \\ K_{pu} & K_{pv} & 0 & 0 & 0 \\ & & & & \end{bmatrix} \begin{Bmatrix} \Delta u \\ \Delta v \\ \Delta\sigma \\ \Delta p \end{Bmatrix} = -\begin{Bmatrix} F_{\alpha^u} \\ F_{\alpha^v} \\ F_{\alpha\sigma} \\ F_{\alpha^p} \end{Bmatrix} \quad (27)$$

Where,

$K_{uu} = Re(K_{\alpha\beta\gamma^x}U_\gamma + K_{\alpha\gamma\beta^x}U_\gamma + K_{\alpha\beta\gamma^y}V_\beta) + (1-\lambda)\left(S_{\alpha\beta^{xx}} + S_{\alpha\beta^{yy}}\right)$
$K_{uv} = K_{\alpha\beta\gamma^y}U\gamma$, $K_{uT} = -K_{\alpha\beta^x} - K_{\alpha\beta^y}$, $K_{up} = M_{\alpha\mu^x}K_{vu} = K_{\alpha\beta\gamma^x}V\gamma$,
$K_{vv} = Re(K_{\alpha\beta\gamma^x}U_\beta + K_{\alpha\gamma\beta^x}V_\gamma + K_{\alpha\gamma\beta^y}V_\gamma) + (1-\lambda)\left(S_{\alpha\beta^{xx}} + S_{\alpha\beta^{yy}}\right)$
$K_{v\sigma} = -K_{\alpha\beta^x} - K_{\alpha\beta^y}$, $K_{vp} = M_{\alpha\mu^y}$, $K_{\sigma u} = W_i K_{\alpha\beta\gamma^x}\sigma_c - K_{\alpha\beta^x}\mu_v$,
$K_{\sigma v} = W_i K_{\alpha\beta\gamma^y}\sigma_c - K_{\alpha\beta^y}\mu_v$, $K_{\sigma\sigma} = K_{\alpha\beta} - 2W_i(K_{\alpha\beta\gamma^x}U_c + K_{\alpha\beta\gamma^y}U_c)$
$K_{\sigma p} = 0, K_{pu} = K_{\alpha\beta^x}, K_{pv} = K_{\alpha\beta^y}, K_{p\sigma} = 0 = K_{pp}.$
$K_{\theta\theta} = RePr(K_{\alpha\beta\gamma^x}U_\beta + K_{\alpha\beta\gamma^y}V_\beta) + (S_{\alpha\beta^{xx}} + S_{\alpha\beta^{yy}}) + \rho_f K_{\alpha\beta}$
$K_{\theta u} = K_{\alpha\beta\gamma^x}\theta\gamma, K_{\theta v} = K_{\alpha\beta\gamma^y}\theta\gamma, K_{\sigma\theta} = K_{\theta\sigma} = 0$
$K_{\theta p} = 0$, $K_{pu} = K_{\alpha\beta^x}$ $K_{p\theta} = 0 = K_{pp}, K_{pv} = K_{\alpha\beta^y}$

V. Numerical Results

The main aim of this mathematical model is to know and bring out the effects of aneurysmatic artery having various conditions. The various aneurysmal arterial models are considered for the study such as (i) if both aneurysms are 50 percent bulge compared to normal blood artery (ii) If first one is twice of second aneurysm (iii) if second one is twice of 1st aneurysm and (iv) if both aneurysm is 100% bulge compared to normal blood artery. In this research, we are concerned with non-Newtonian fluids type, with the flows of incompressible viscoelastic Oldroyd-B fluids. It is very significant to select the blood viscosity for precision of simulation of blood flows. the generalized Cross model, the parabolic velocity equation and the corresponding extra stresses components are used for shear-thinning properties of blood.

A validation test has done [11] to evaluate the correctness of the numerical simulation and blood flow visualization for Oldroyd-B case. It has computed blood velocity, pressure and streamlins with dimensionless numbers *Wi* and *Re* for considered model. For this numerical study, the following blood properties are considered: $0 \le Wi \le 1$, $0 < Re \le 3000$, $\mu_0 = 0.16$ Pa.s, $\mu_n = 0.0036$ Pa.s, a = 1.23,b = 0.64, $\lambda = 8.2$s, $\rho = 1050$ kg.m-3, $l_0 = 2R$, l= 10R, R= 3.1mm, and $l_a = 6R$.

The main objective of this work is to discuss the effects of various aneurysmatic artery conditions and dimensionless numbers, *Re* on blood flow. The blood simulation has shown in bellows in terms of axial velocity contour lines.

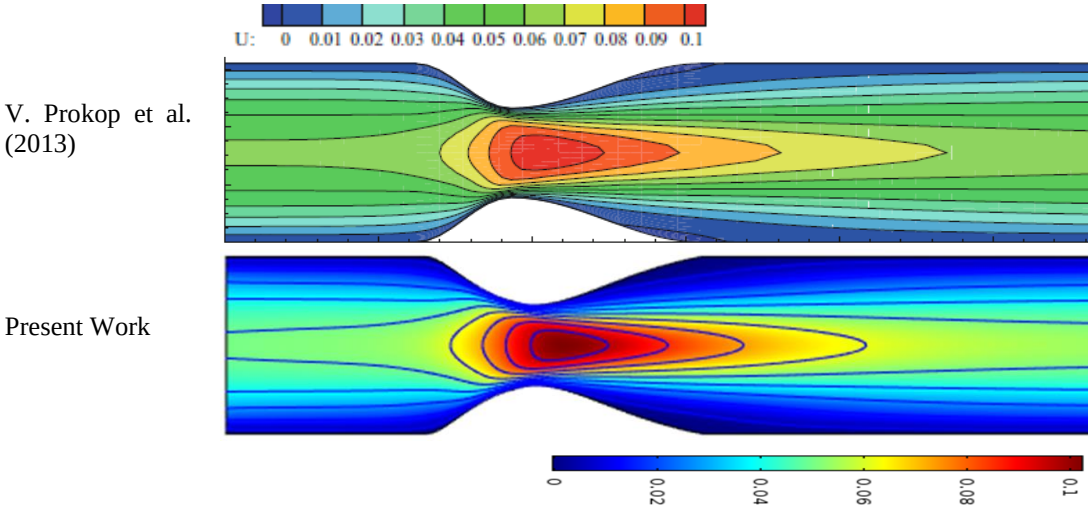

Figure 3: Comparison of velocity contour of blood flow through stenosis artery

The impact of Aneurysmal artery on blood flow

The simulation of blood flow is shown in the Figures 4-5 in term of vector contour lines and streamlines for (a) Case-1(50% aneurysm) (b) case-2 (1st aneurysm is twice of 2nd aneurysm) (c) case -3 (2nd aneurysm is twice of 1st aneurysm) and (d) case-4 (100% aneurysm) with constant flow rate. The study has been done using Oldroyd-B fluid for all four cases. It is very remarkable that the recirculation zones originated at the beginning of the 1st aneurysm for all models. In Figure-4, the size of recirculation zone of case-1 is bigger than case-4 because of the presence of higher aneurysm. It is found that blood flow has decreased in the presence of 100% bulge area in the artery due to the shear-thinning viscosity of blood properties.

In Figure 5, the blood flow simulation has shown with streamlines and vector arrays. The vortexes are found at the area of the bulge in the artery which is an important finding of the work. More vortexes are observed in case-4 at the swell-up region because of low blood velocity. So, the separation regions and backflow of blood have been created at the more aneurysmal artery. These vortexes are indicative of arterial disease due to the existence of a high aneurysmal artery.

The velocity profiles are shown in Figure 6 for all models at Re-1000 and Wi-0.5 numerically. The higher velocity is found for case-1 and the lowest velocity is observed for case-4. At the high swell-up area the velocity has decreased, and the velocity has increased at less bulge region. At the beginning of an aneurysm, the blood velocity is maximum, and the minimum velocity is gained at 2nd aneurysmal artery. The obtained result also agrees with the theoretical result.

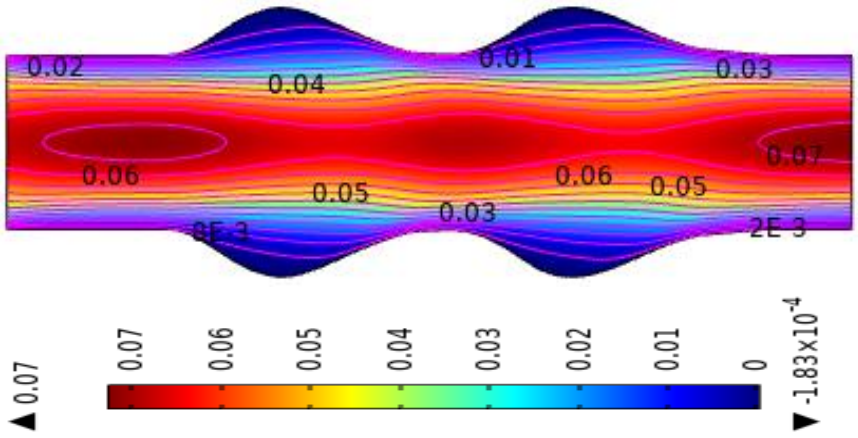

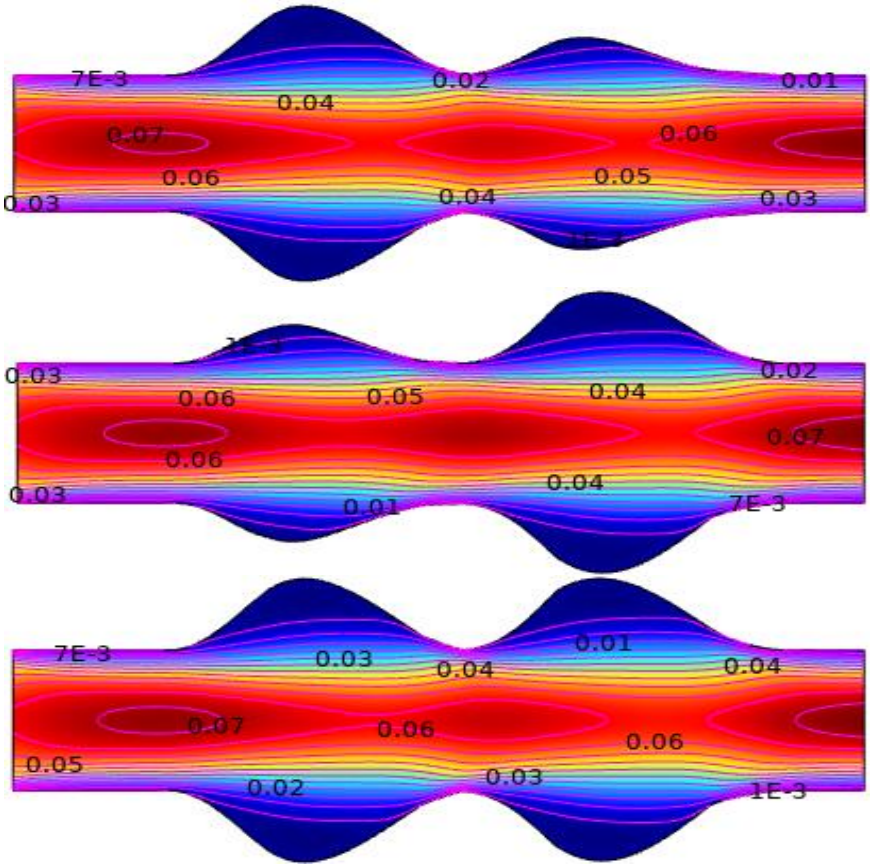

Figure 4: Velocity contour line on blood flow through multiple anuerysmatic arteries with various condition at *Re*=1000 and *Wi* = 0.5

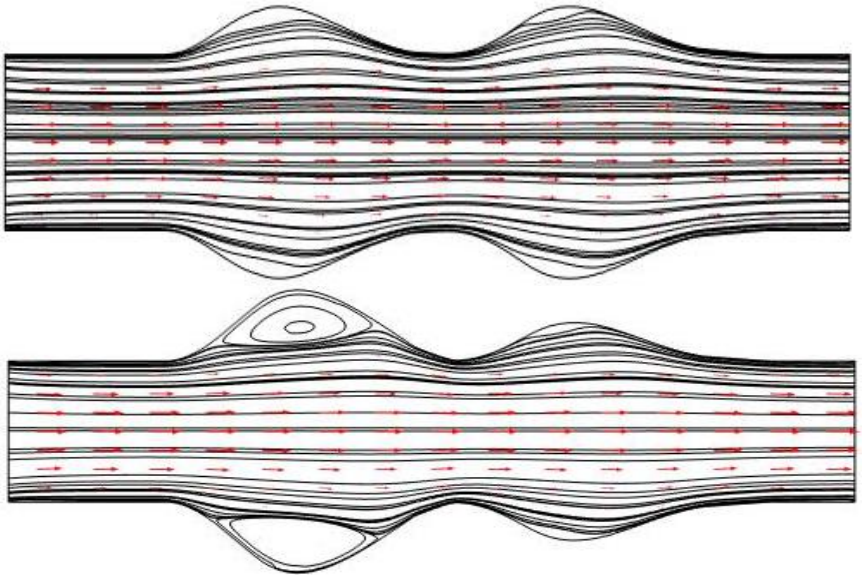

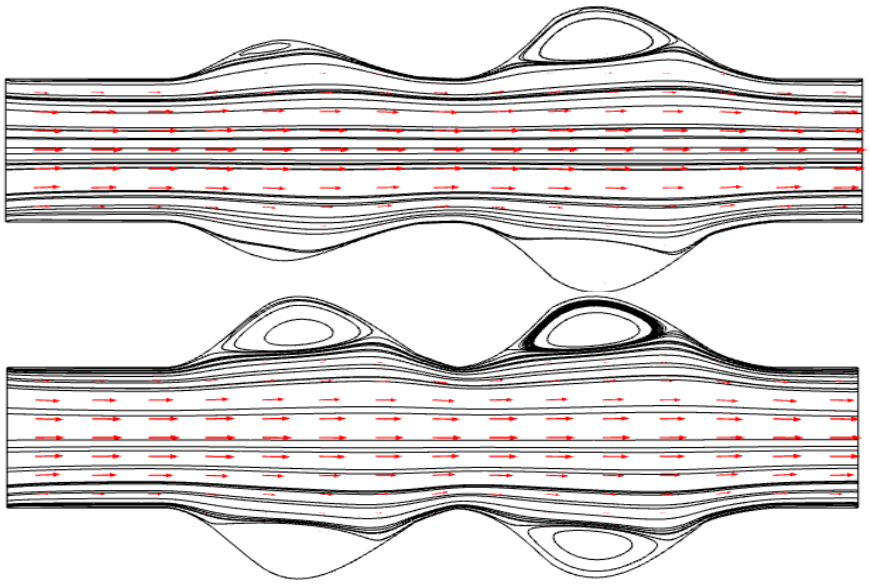

Figure 5: Stream lines with vector array on blood flow through multiple anuerysmatic arteries with various condition at *Re*=1000 and *Wi* = 0.5

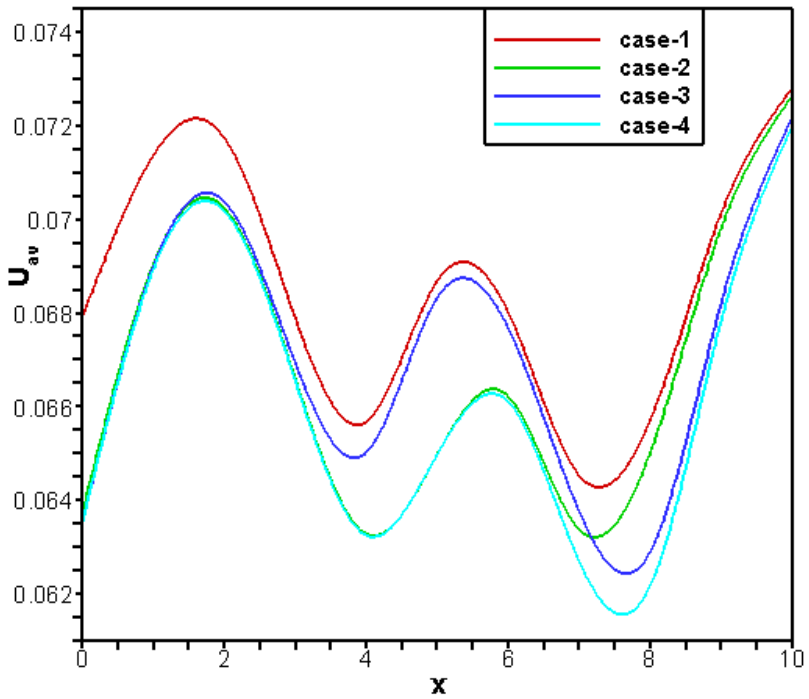

Figure 6: Velocity profile for case-1 (50% aneurysm), case-2 (1st aneurysm is twice of 2nd aneurysm), case-3 (2nd aneurysm is twice of 1st aneurysm), case-4 (100% aneurysm) at Wi=0.5 and Re=1000

Aneurysmal artery effects on pressure distribution

The pressure distribution is presented in Figure 7 in terms of contour lines for all four cases with constant flow rate at Re=1000 and Wi=0.5. In Figure 7, the iso-pressure contours show how to gain a lower value at the separation point and decrease mechanically. The highest value pointed at the reattachment point, which created a stagnation point, and fell suddenly at the beginning of high aneurysm. In the presence of a high bulge region, the pressure has decreased rapidly and gained a minimum value at the outlet in case 4. The flow separation points have migrated towards blood vessels. In the presence of a higher and lower bulge area (case 2) in an artery consecutively then a remarkable change is found for pressure distribution. The pressure gradient is very intensive for case 4, and it changed considerably all over the blood vessel. The important changes have occurred in the more dilating (case 4) area compared to the less dilating region (case 1).

The graphical presentation of pressure profiles is shown in Figure 8 for all cases at Wi=0.6 and Re=1000. The pressure has decreased for all models with respect to the vessel axis. In Figure 8, the maximum and minimum pressure originated at the 1st and 2nd aneurysmal areas respectively for case 4.

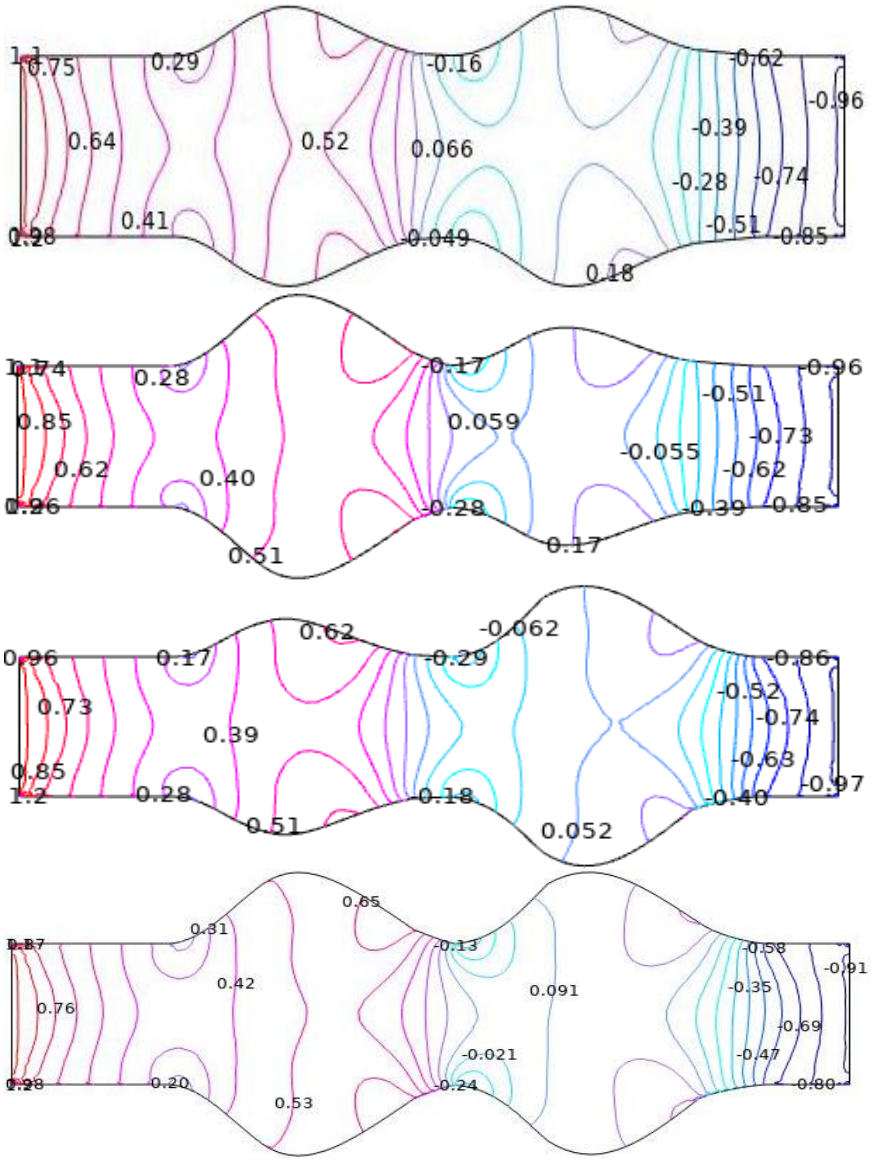

Figure 7: Pressure distribution on blood flow through multiple anuerysmatic arteries with various condition at *Re*=1000 and *Wi* = 0.5

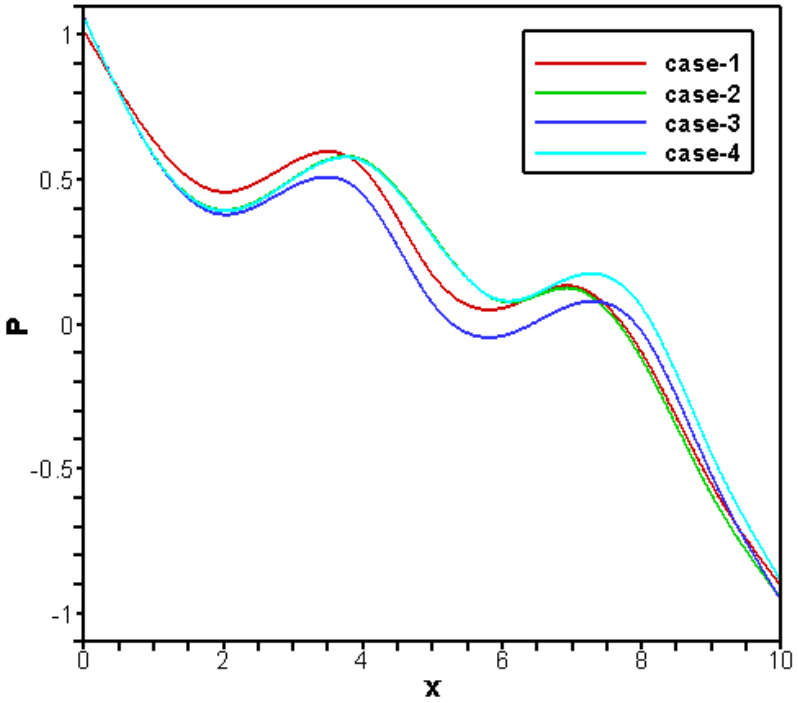

Figure 8: Pressure profile for case-1 (50% aneurysm), case-2 (1st aneurysm is twice of 2nd aneurysm), case-3 (2nd aneurysm is twice of 1st aneurysm), case-4 (100% aneurysm) at Wi=0.5 and Re=1000

Effects of Re on blood flow

The effect of Reynold numbers ($0 < Re \leq 3000$) on blood flow are shown in Figures 9-12 for all models with $Wi = 0.6$ and constant flow rate. The different Re is computed on the based on the blood density, blood viscosity, length of the model and various velocity at inlet.

The permanent recirculation zones are created at various regions of models for Re-1 and 1000 for all cases. At Re=1, the flow patterns are symmetric about the vessel axis for case 1 and case 4 but vortexes have produced for case 2. So, it indicates the blood flow disorder is more in case 2. The blood flow has decreased compared to the less dilating area to high dilating regions for Re=1. The blood flow patterns have changed rapidly due to excess aneurysms in the artery which is an important outcome of this study. With the increase of Re the blood flow has decreased due to the existence of aneurysmal artery for all cases. In Figure 12, the flow patterns have changed more, and vortexes are found for case 4 which is inferred to be arterial diseases due to the presence of excess aneurysm.

The velocity profiles are shown in Figure 13 for all models with various Re graphically. The values of velocity 0.061, 0.066, 0.065, and 0.064 are found for Re=1, 1000, 2000, and 3000 respectively in case 1 at the first aneurysm. On the other hand, in case 4, the velocities are 0.052, 0.063, 0.062, and 0.061 for Re=1, 1000, 2000, and 3000 respectively at the first aneurysm. It is found that 14.47 percent is the highest deviation of velocity at Re=1 due to more aneurysmatic artery and the minimum deviation is 2.83 percent for Re-1000. It is an important outcome that the velocity has gained a lower value for the presence of a more dilating region.

The pressure contour plots are illustrated in Figures 14 to 17 for various Reynold numbers (*Re*=1, 1000, 2000 & 3000). At the beginning of the models the pressure patterns gained maximum value and decreased gradually. The minimum and maximum values are found at upstream and downstream respectively. At reattachment point, the pressure has gained lower value for Re=3000 and the lowest value is found for case 4 which infers the arterial diseases.

The most influential of the models on the pressure distribution is found for case 4 and the high dilating area. The pressure contour lines are travelling to upper vessel wall with the increase of Reynold number. The pressure distribution of blood flow has changed dramatically and produces the lowest value at the high aneurysmal artery.

In Figure 18, A remarkable variation has appeared for blood pressure at Reynolds number, *Re*=3000, and pressure is intensified. The pressure has increased with the increase of aneurysm of the artery. The lowest value is -0.32 in the dilating region for case 4 at Re = 3000. On the other hand, the highest value is 0.56 for case 1 at Re=1. The pressure has decreased with the increase of Re along with the vessel axis. The pressure variation has indicated arterial diseases in the blood vessel which is an important finding of this study.

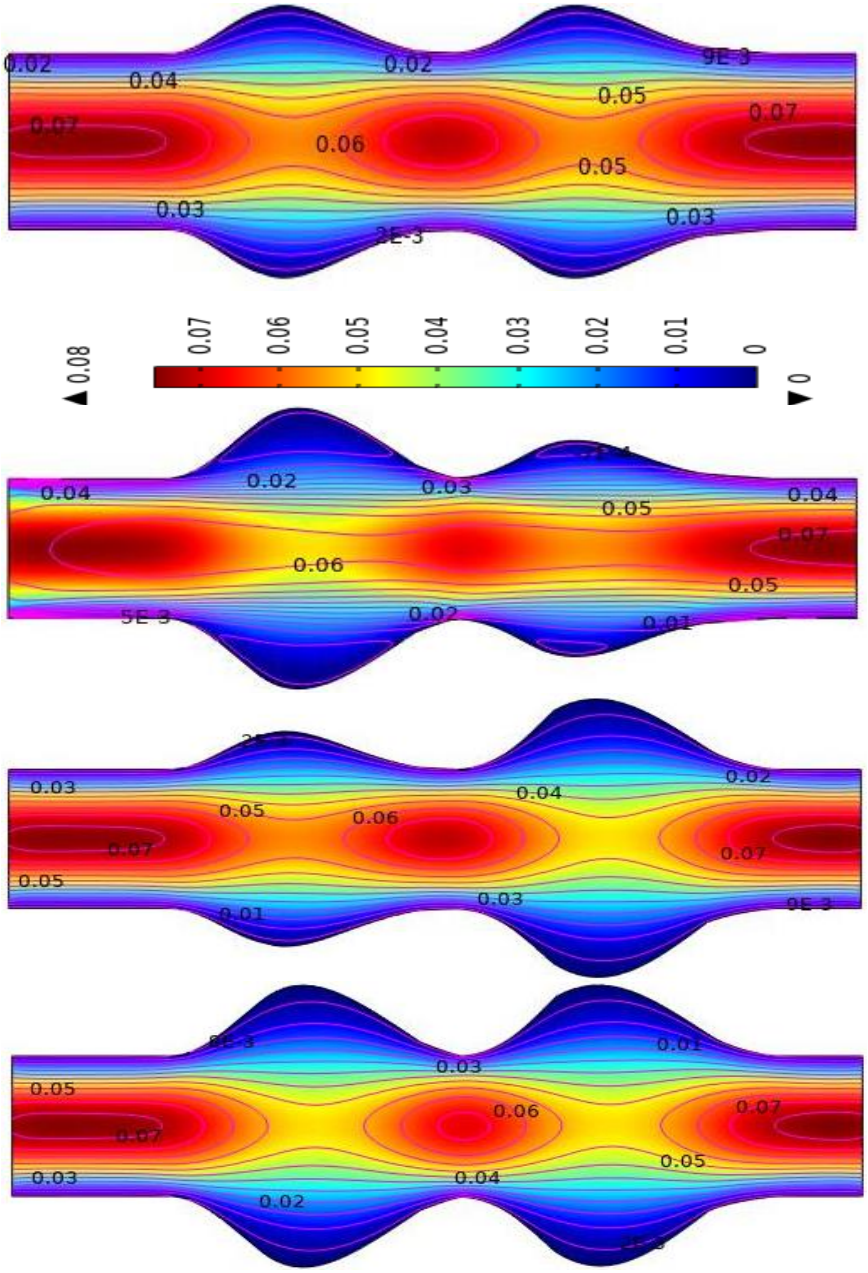

Figure 9: Velocity contour line on blood flow through multiple anuerysmatic arteries with various condition at *Re*=1 and *Wi* = 0.5

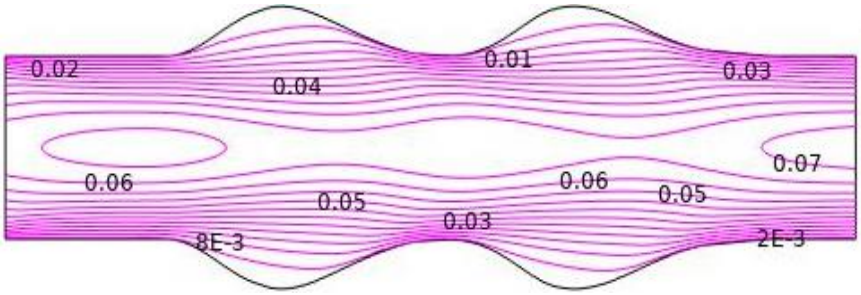

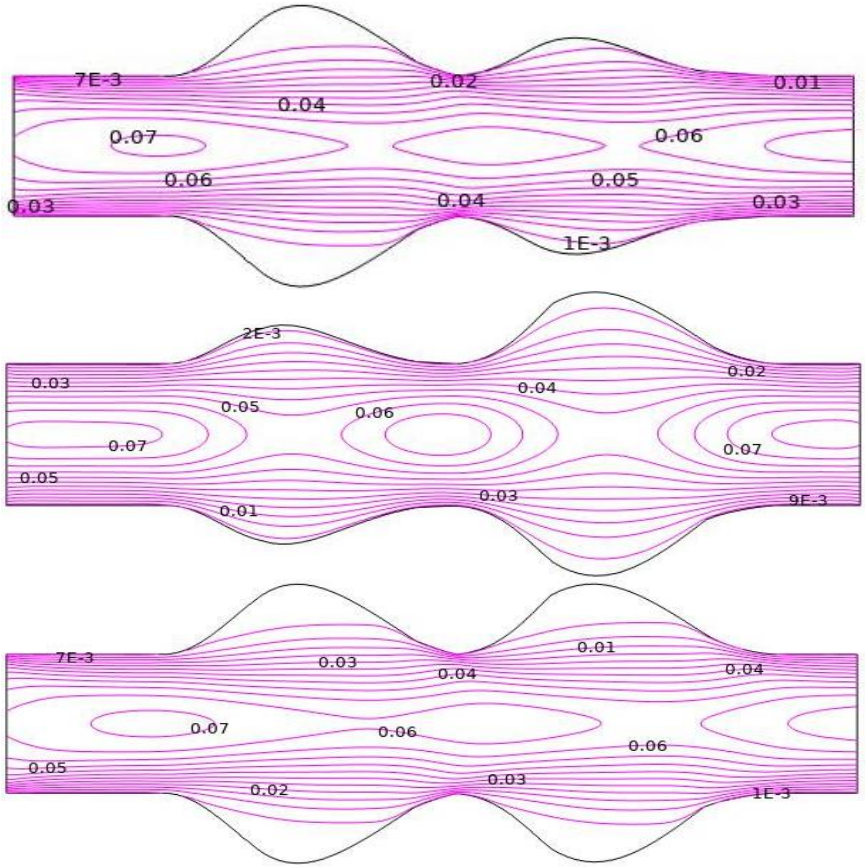

Figure 10: Velocity contour line on blood flow through multiple anuerysmatic arteries with various condition at *Re*=1000 and *Wi* = 0.5

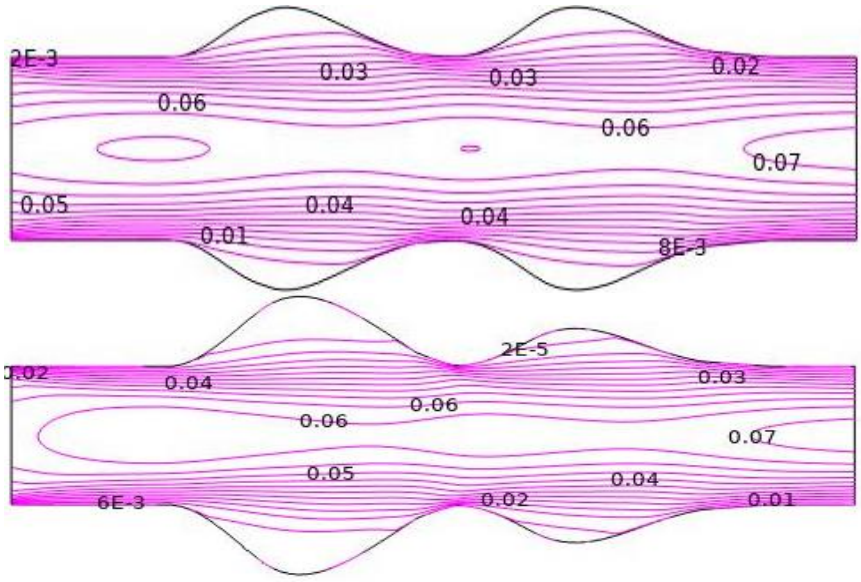

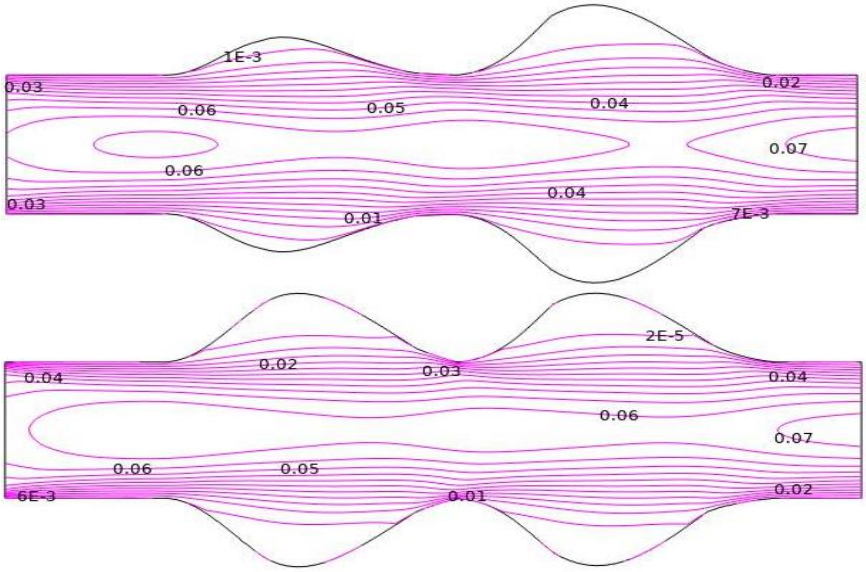

Figure 11: Velocity contour line on blood flow through multiple anuerysmatic arteries with various condition at *Re*=2000 and *Wi* = 0.5

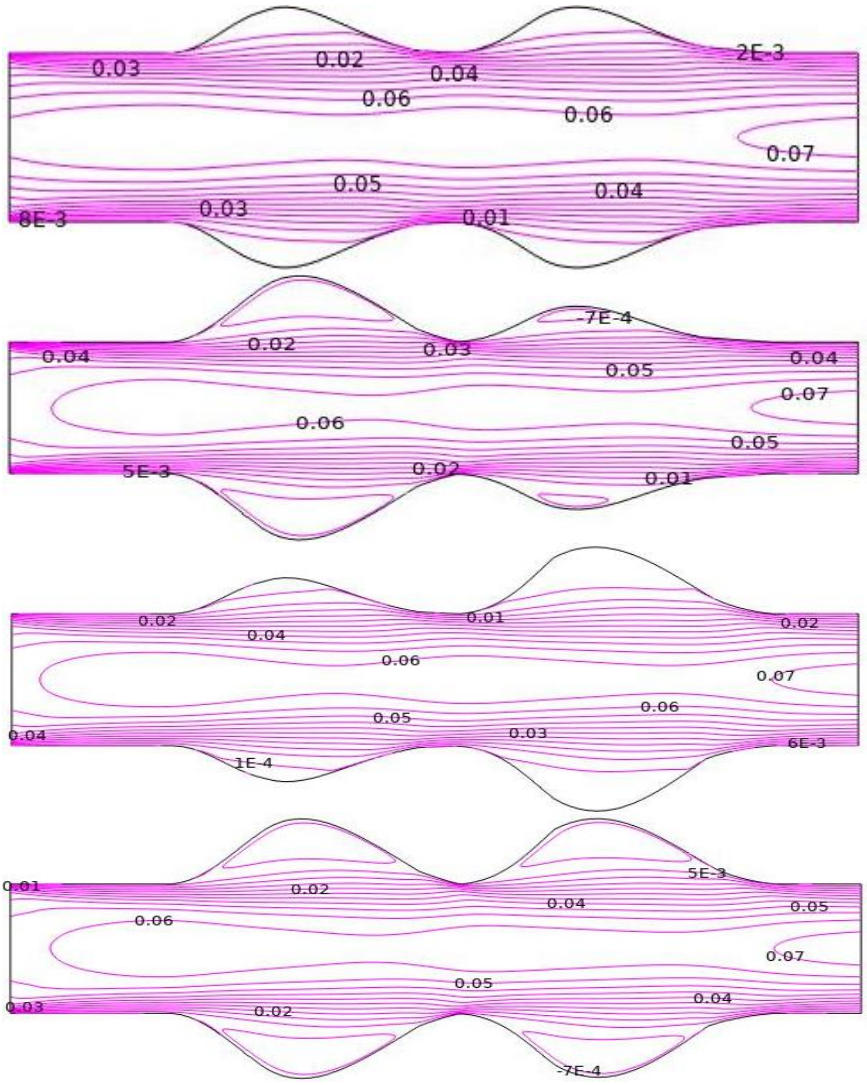

Figure 12: Velocity contour line on blood through multiple anuerysmatic arteries with various condition at *Re*=3000 and *Wi* = 0.5

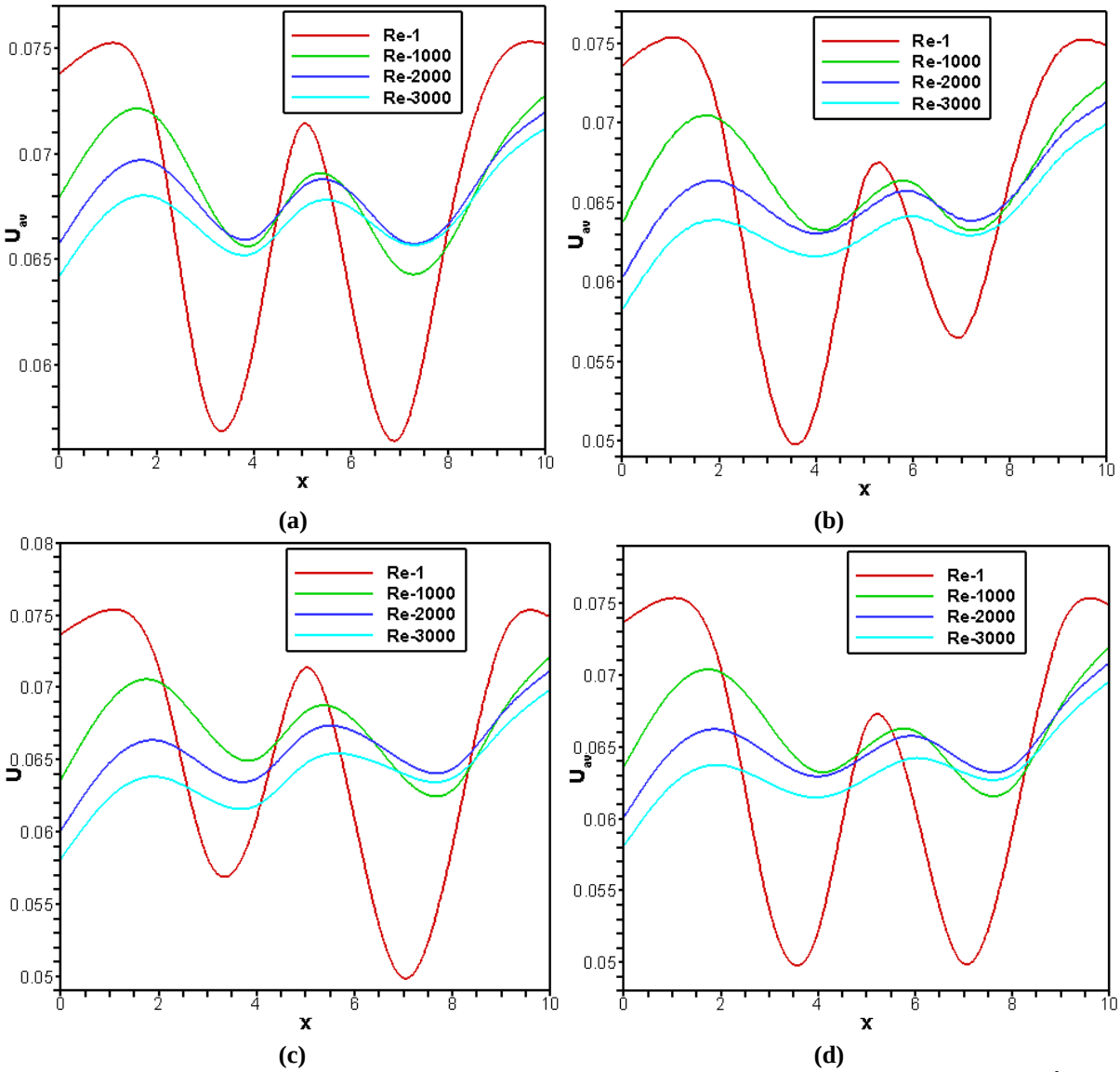

Figure 13: Velocity profile for a. case-1 (50% aneurysm), b. case-2 (1st aneurysm is twice of 2nd aneurysm), c. case-3 (2nd aneurysm is twice of 1st aneurysm), d. case-4 (100% aneurysm) at Wi=0.5 and Re=1000.

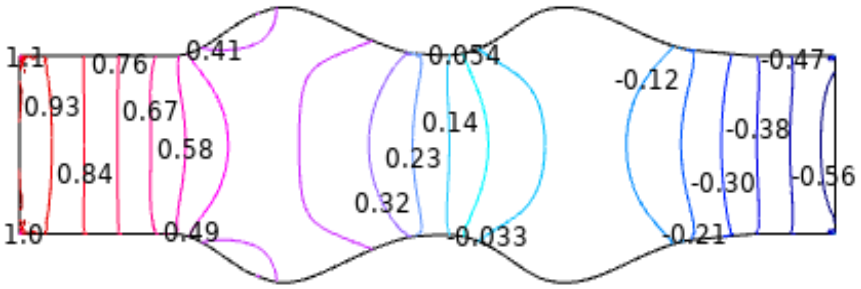

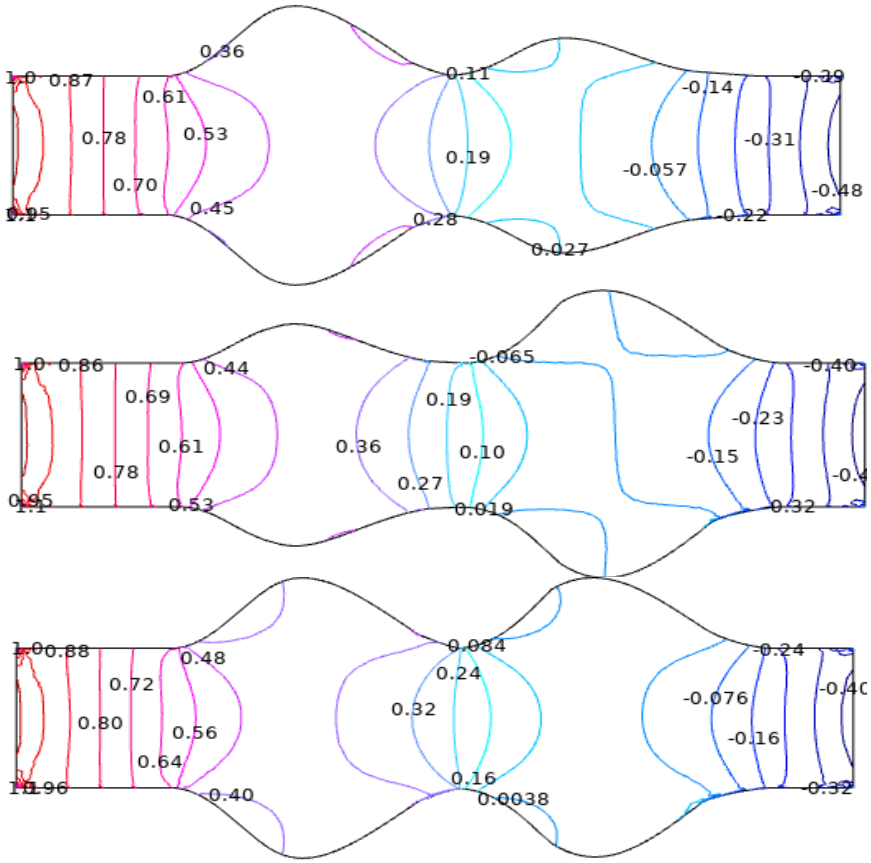

Figure 14: Pressure contour line on blood flow through multiples anuerysmatic arteries with various condition at *Re*=1 and *Wi* = 0.5

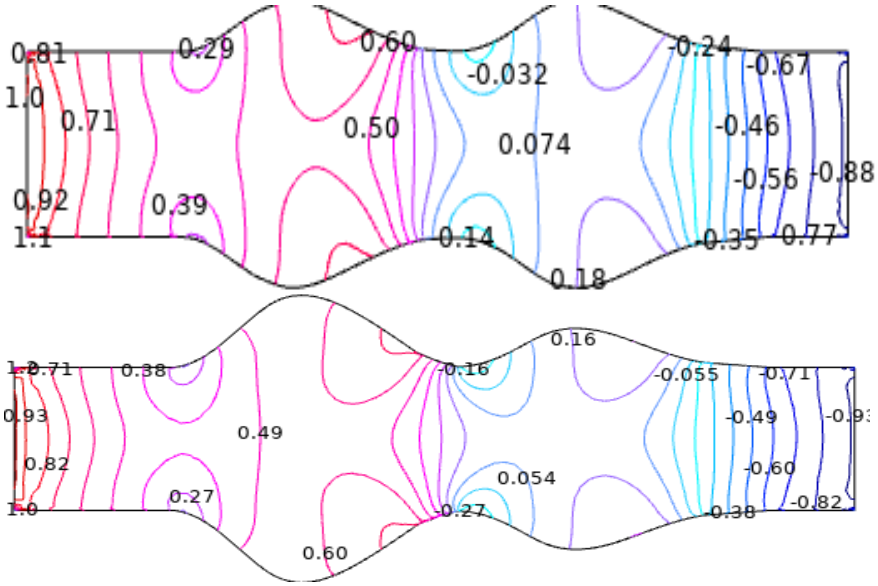

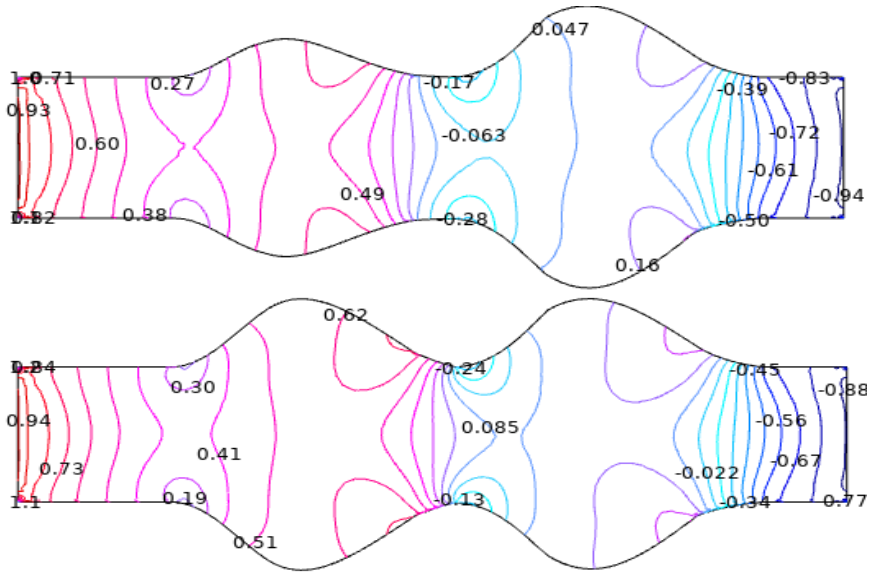

Figure 15: Pressure contour line on blood flow through multiples anuerysmatic arteries with various condition at *Re*=1000 and *Wi* = 0.5

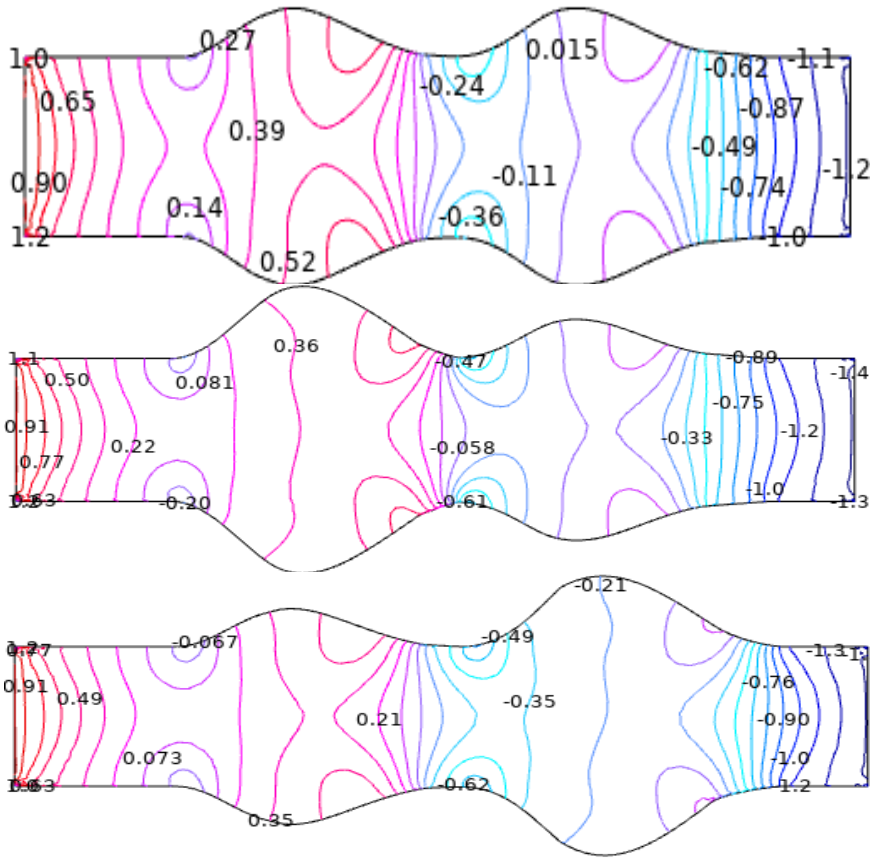

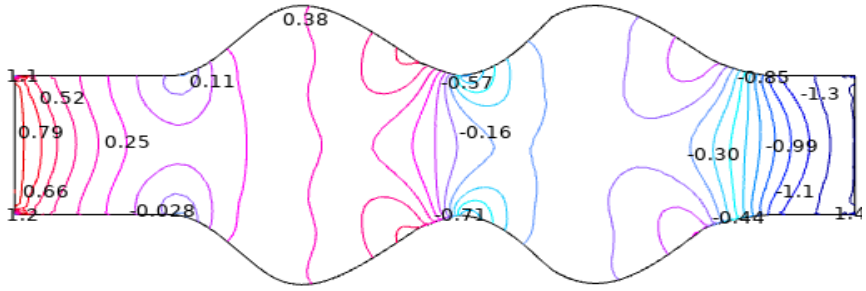

Figure 16: Pressure contour line on blood flow through multiples anuerysmatic arteries with various condition at *Re*=2000 and *Wi* = 0.5

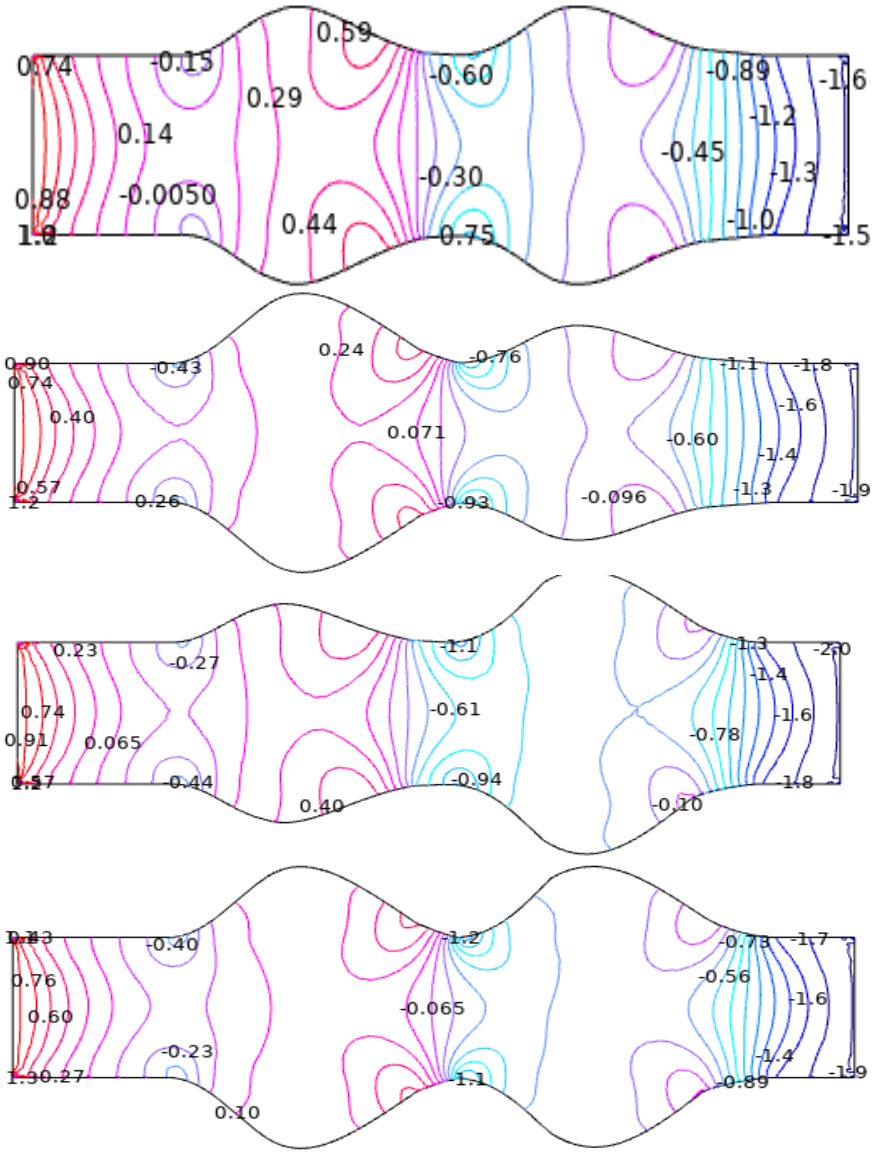

Figure 17: Pressure contour line on blood flow through multiples anuerysmatic arteries with various condition at *Re*=3000 and *Wi* = 0.5

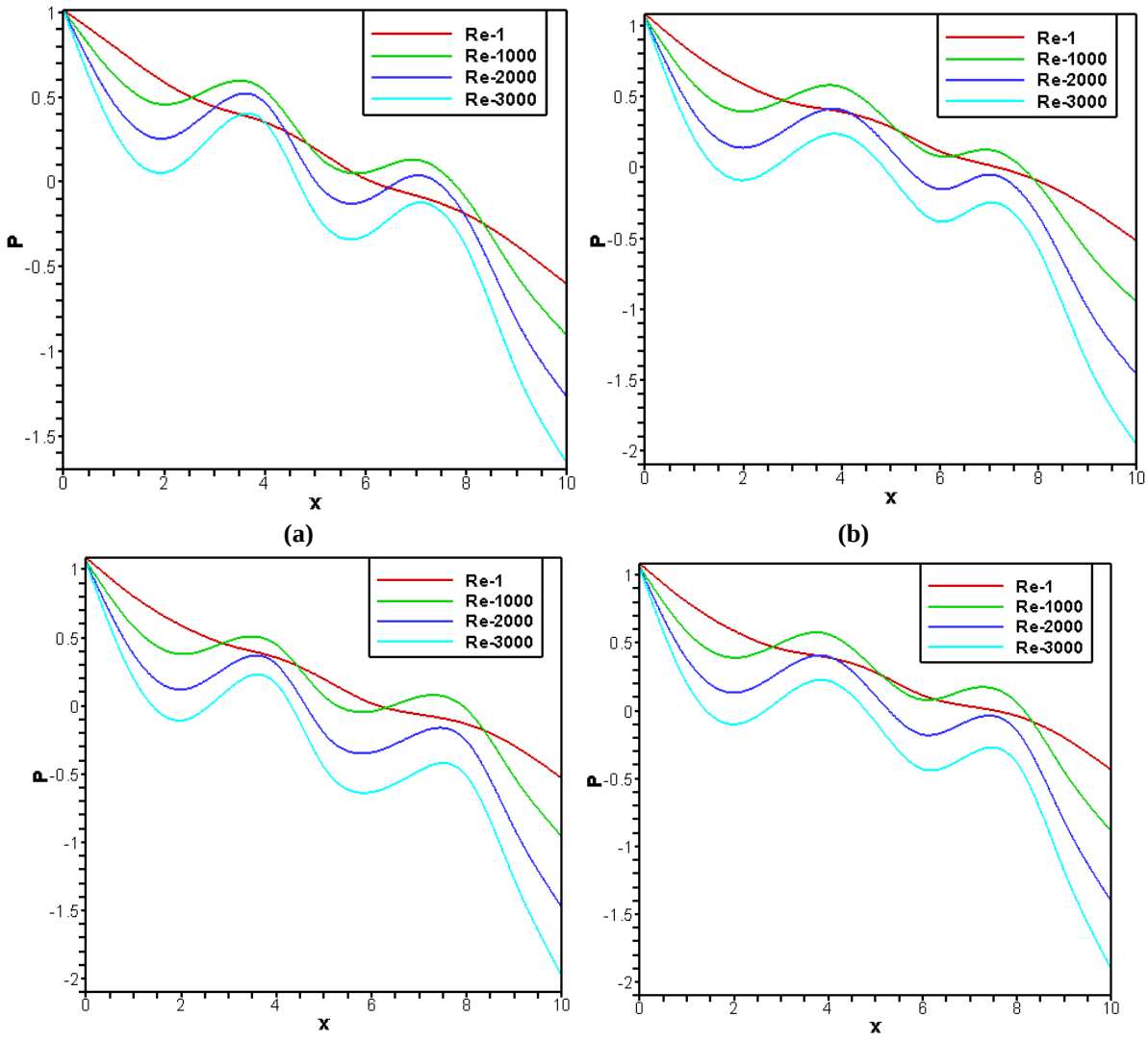

Figure 18: Pressure profile for (a). case-1 (50% aneurysm), (b). case-2 (1st aneurysm is twice of 2nd aneurysm), (c). case-3 (2nd aneurysm is twice of 1st aneurysm), (d). case-4 (100% aneurysm) at Wi=0.5 and Re=1000.

VI. Conclusion

The finite element method is applied to simulate the blood flow through various aneurysm arteries. The Oldroyd-B model is used for blood flow analysis due to shear-thinning and blood viscosity. This model plays an essential role in finding blood flow variables. The numerical study is performed to investigate the blood flow patterns through aneurysm in steady flow for all cases. The blood flow variables are changed for all models along the vessel axis at the aneurysm. The depth of aneurysm and blood viscosity are the main reasons for Newtonian and Non-Newtonian solutions. At the present problems, the finite element method and the Newton-Raphson iteration method are used to solve the governing equations for the nodal velocity component, tensor component, and pressure by considering Weissenberg numbers (Wi=0.5) and Reynolds numbers of 1 to 3×10^3.

The effect of an aneurysmal artery on blood flow has been studied for various values of relevant parameters. Numerical models and simulations provide an effective non-invasive technique to obtain accurate data on blood flow in human arteries and appropriate identification of arterial diseases. The following outcomes may be concluded from the present study:

i. Significant changes in blood flow characteristics at various aneurysm conditions for all cases are found in this investigation. The blood velocity has reduced due to the presence of a 100% aneurysm is an important finding.

ii. The lowest value of blood velocity is found at 100% dilating area in the 2nd aneurysm for case 4. On the contrary, the highest velocity is observed at 50% bulge region for case 1.

iii. The maximum and minimum values of pressure are found at 100% and 50 % aneurysmal artery respectively.
iv. The effect of Reynold numbers (Re) are significant at dilating area and blood flow variables have changed dramatically for 100% aneurysm.
v. The pressure patterns have decreased with the increase of Re for all cases the highest value is found in case 4.
vi. Oval types of recirculation zone originated at the beginning of the aneurysm regions for Re=1 and 1000.

Acknowledgements

We are grateful to the Bangladesh University of Professionals (BUP) to give all services during the research.

References

[1] M. Anand and K. R. Rajagopal, "A shear-thinning viscoelastic fluid model for describing the flow of blood," Int. J. Cardiovasc. Med. Sci., vol. 4, no. 2, pp. 59–68, 2004.
[2] T. W. Secomb, "Hemodynamics," Compr. Physiol., vol. 6, no. 2, pp. 975–1003, 2016, doi: 10.1002/cphy.c150038.
[3] C. Tu and M. Deville, "Pulsatile flow of Non-Newtonian fluids through arterial stenoses," J. Biomech., vol. 29, no. 7, pp. 899–908, 1996, doi: 10.1016/0021-9290(95)00151-4.
[4] R. Keslerová and K. Kozel, "Numerical solution of viscous and viscoelastic fluids flow through the branching channel by finite volume scheme", J. Phys.: Conf. Ser. 633(2015)012128.
[5] R. Budwig, O. Elger, H. Hooper, and J. Slippy, "Steady flow in abdominal aortic aneurysm models," J. Biomech. Eng., vol. 115, no. 4, pp. 418–423, 1993, doi: 10.1115/1.2895506.
[6] E. A. Finol and C. H. Amon, "Blood flow in abdominal aortic aneurysms: Pulsatile flow hemodynamics," J. Biomech. Eng., vol. 123, no. 5, pp. 474–484, 2001, doi: 10.1115/1.1395573.
[7] G. Mistelbauer et al., "Semi-automatic vessel detection for challenging cases of peripheral arterial disease," Comput. Biol. Med., vol. 133, no. December 2020, 2021, doi: 10.1016/j.compbiomed.2021.104344.
[8] I. Güler and E. D. Übeyli, "Detection of ophthalmic arterial doppler signals with Behcet disease using multilayer perceptron neural network," Comput. Biol. Med., vol. 35, no. 2, pp. 121–132, 2005, doi: 10.1016/j.compbiomed.2003.12.007.
[9] C. Tu, M. Deville, L. Dheur, and L. Vanderschuren, "Finite element simulation of pulsatile flow through arterial stenosis," J. Biomech., vol. 25, no. 10, pp. 1141–1152, 1992, doi: 10.1016/0021-9290(92)90070-H.
[10] M. D'Elia, M. Perego, and A. Veneziani, "A variational data assimilation procedure for the incompressible navier-stokes equations in hemodynamics," J. Sci. Comput., vol. 52, no. 2, pp. 340–359, 2012, doi: 10.1007/s10915-011-9547-6.
[11] V. Prokop and K. Kozel, "Numerical Mathematics and Advanced Applications 2011," Numer. Math. Adv. Appl. 2011, 2013, doi: 10.1007/978-3-642-33134-3.
[12] T. Guerra, J. Tiago, and A. Sequeira, "Optimal control in blood flow simulations," Int. J. Non. Linear. Mech., vol. 64, pp. 57–69, 2014, doi: 10.1016/j.ijnonlinmec.2014.04.005.
[13] J. Bernsdorf and D. Wang, "Non-Newtonian blood flow simulation in cerebral aneurysms," Comput. Math. with Appl., vol. 58, no. 5, pp. 1024–1029, 2009, doi: 10.1016/j.camwa.2009.02.019.
[14] S. Mukhopadhyay and G. C. Layek, "Analysis of blood flow through a modelled artery with an aneurysm," Appl. Math. Comput., vol. 217, no. 16, pp. 6792–6801, 2011, doi: 10.1016/j.amc.2010.10.011.
[15] K. M. Prasad, T. Sudha, and M. V. Phanikumari, "Investigation of blood flow through an artery in the presence of overlapping stenosis," J. Nav. Archit. Mar. Eng., vol. 14, no. 1, pp. 38–46, 2017, doi: 10.3329/jname.v14i1.31165.
[16] J. Febina, M. Y. Sikkandar, and N. M. Sudharsan, "Wall Shear Stress Estimation of Thoracic Aortic Aneurysm Using Computational Fluid Dynamics," Comput. Math. Methods Med., vol. 2018, 2018, doi: 10.1155/2018/7126532.
[17] Y. G. Stergiou, A. G. Kanaris, A. A. Mouza, and S. V. Paras, "Fluid-structure interaction in abdominal aortic aneurysms: Effect of haematocrit," Fluids, vol. 4, no. 1, 2019, doi: 10.3390/fluids4010011.
[18] L. Sheh Hong, M. Azrul Hisham Mohd Adib, M. Uzair Matalif, M. Shafie Abdullah, N. Hartini Mohd Taib, and R. Hassan, "Modeling and Simulation of Blood Flow Analysis on Simplified Aneurysm Models," IOP Conf. Ser. Mater. Sci. Eng., vol. 917, no. 1, 2020, doi: 10.1088/1757-899X/917/1/012067.
[19] N. S. Shafii et al., "Hemodynamic and Flow Recirculation Effect on Rupture Prediction of Middle Cerebral Artery Aneurysm," J. Adv. Res. Fluid Mech. Therm. Sci., vol. 79, no. 1, 2020, doi: 10.37934/arfmts.79.1.116.
[20] N. Najihah Mohd Nazri, M. Uzair Matalif, and M. Azrul Hisham Mohd Adib, "Effects of blood flow patent and cross-sectional area on hemodynamic into patient-specific cerebral aneurysm via fluid-structure interaction method: A review," in IOP Conference Series: Materials Science and Engineering, 2020, vol. 788, no. 1. doi: 10.1088/1757-899X/788/1/012022.
[21] M. Lindquist Liljeqvist, M. Bogdanovic, A. Siika, T. C. Gasser, R. Hultgren, and J. Roy, "Geometric and biomechanical modeling aided by machine learning improves the prediction of growth and rupture of small abdominal aortic aneurysms," Sci. Rep., vol. 11, no. 1, pp. 1–10, 2021, doi: 10.1038/s41598-021-96512-3.
[22] M. N. Uddin, M. A. Alim, M. M. Karim, and M. M. Alam, "Effect of aneurysmatic artery on blood flow having permeability in human organ," J. Nav. Archit. Mar. Eng., vol. 18, no. 2, pp. 155–173, Dec. 2021, doi: 10.3329/jname.v18i2.53624.
[23] X. Y. Shen, M. B. Gerdroodbary, A. Poozesh, A. Musa Abazari, and S. M. Imani, "Effects of blood flow characteristics on rupture of cerebral aneurysm: Computational study," Int. J. Mod. Phys. C, vol. 32, no. 11, 2021, doi: 10.1142/S0129183121501436.
[24] X. Y. Shen, H. Q. Xu, M. B. Gerdroodbary, S. Valiallah Mousavi, A. Musa Abazari, and S. M. Imani, "Numerical simulation of blood flow effects on rupture of aneurysm in middle cerebral artery," Int. J. Mod. Phys. C, vol. 33, no. 3, 2022, doi: 10.1142/S0129183122500309.
[25] M. N. Uddin, M. M. Uddin, and M. M. Alam, "Comparative Mathematical Study of Blood Flow Through Stenotic and Aneurysmatic Artery with the Presence and Absence of Blood Clots," Malaysian J. Math. Sci., vol. 16, no. 3, pp. 599–623, 2022, doi: 10.47836/mjms.16.3.12.
[26] V. P. Srivastava and R. Rastogi, "Blood flow through a stenosed catheterized artery: Effects of hematocrit and stenosis shape," Comput. Math. with Appl., vol. 59, no. 4, pp. 1377–1385, 2010, doi: 10.1016/j.camwa.2009.12.007.
[27] UF Health aortic disease center, https://ufhealth.org/uf-health-aortic-disease-center/thoracoabdominal-aortic-aneurysm. Accessed: 2023-04-10.
[28] I. R. Jamil and M. Humaira, "Modeling and predicting blood flow characteristics through double senosed artery from computational

fluid dynamics simulations using deep learning models," Int. J. Adv. Comput. Sci. Appl., vol. 13, no. 1, pp. 832–841, 2022, doi: 10.14569/IJACSA.2022.0130197.
[29] C. Yang and Z. Mao, "Numerical simulation of viscous flow of a non-newtonian fluid," 3rd Int. Conf. CFD Miner. Process Ind., no. December, pp. 391–396, 2003.
[30] R. G. Owens and T. N. Phillips, Computational Rheology. 2010. doi: 10.1142/9781860949425.
[31] N. Arada, M. Pires, and A. Sequeira, "Numerical simulations of shear-thinning Oldroyd-B fluids in curved pipes," IASME Trans., 2005,
[32] R. K. Dash, G. Jayaraman, and K. N. Mehta, "Flow in a catheterized curved artery with stenosis," J. Biomech., vol. 32, no. 1, 1999, doi: 10.1016/S0021-9290(98)00142-0.
[33] H. Saunders, "Finite element methods—An introduction," Finite Elem. Anal. Des., vol. 3, no. 4, pp. 360–361, 1987, doi: 10.1016/0168-874x(87)90019-9.
[34] Comsol Multiphysics 5.3. https://cdn.comsol.com/doc/4.3a/COMSOL_ReleaseNotes.pdf. Accessed: 2023-3-20.
[35] M. K. Ahirwal, A. Kumar, and G. K. Singh, Basics of Matlab Programming, no. October. 2021. doi: 10.1007/978-3-030-67098-6_5.
[36] S.S.Rao, The Finite Element Method in Engingeering, Elsevier Science & Technology, 2004. ISBN: 0750678283
[37] O. C. Zienkiewicz, R. L. Taylor, and J. M. Too, "Reduced integration technique in general analysis of plates and shells," Int. J. Numer. Methods Eng., vol. 3, no. 2, pp. 275–290, 1971, doi: 10.1002/nme.1620030211.
[38] T. R. Chandrupatla and A. D. Belegundu, Introduction to finite elements in engineering, 2002, Prentice Hall, New Jersey.